



# CHORUS

This is the accepted manuscript made available via CHORUS. The article has been published as:

## Cascades between Light and Heavy Fermions in the Normal State of Magic-Angle Twisted Bilayer Graphene

Jian Kang, B. Andrei Bernevig, and Oskar Vafek

Phys. Rev. Lett. **127**, 266402 — Published 23 December 2021

DOI: [10.1103/PhysRevLett.127.266402](https://doi.org/10.1103/PhysRevLett.127.266402)

# Cascades between light and heavy fermions in the normal state of magic angle twisted bilayer graphene

Jian Kang,<sup>1,\*</sup> B. Andrei Bernevig,<sup>2</sup> and Oskar Vafek<sup>3,4,†</sup>

<sup>1</sup>*School of Physical Science and Technology & Institute for Advanced Study, Soochow University, Suzhou, 215006, China*

<sup>2</sup>*Department of Physics, Princeton University, Princeton, NJ 08544, USA*

<sup>3</sup>*National High Magnetic Field Laboratory, Tallahassee, Florida, 32310, USA*

<sup>4</sup>*Department of Physics, Florida State University, Tallahassee, Florida 32306, USA*

We present a framework for understanding the cascade transitions and the Landau level degeneracies of twisted bilayer graphene. The Coulomb interaction projected onto narrow bands causes the charged excitations at an integer filling to disperse, forming new bands. If the excitation moves the filling away from the charge neutrality point, then it has a band minimum at the moire Brillouin zone center with a small mass that compares well with the experiment; if towards the charge neutrality point, then it has a much larger mass and a higher degeneracy. At a non-zero density away from an integer filling the excitations interact. The system on the small mass side has a large bandwidth and forms a Fermi liquid. On the large mass side the bandwidth is narrow, the compressibility is negative and the Fermi liquid is likely unstable. This explains the observed sawtooth features in compressibility, the Landau fans pointing away from charge neutrality and their degeneracies. The framework sets the stage for superconductivity at lower temperatures.

The discovery of the correlated insulating phases and superconductivity in the magic-angle twisted bilayer graphene has generated a flurry of research activity [1–76]. This remarkable system exhibits correlated insulating phases at integer fillings of narrow bands [2–6, 8], a hallmark of strong coupling physics. Away from (certain) integer fillings, the same system becomes superconducting below a sufficiently low temperature, descending from a normal state exhibiting Fermi liquid-like quantum oscillations, both hallmarks of charge itineracy.

Recent observations of the cascade transitions in the compressibility and scanning tunneling microscopy studies at temperatures above the full onset of insulation or superconductivity [14, 15, 19] have further sharpened this dichotomy. On the one hand, clear features associated with an integer filling of the moire unit cell were observed as expected in strong coupling [7, 9]. On the other hand, the electron system appears highly compressible when integer filling is approached from the charge neutrality point (CNP) side – even with negative compressibility – and much less compressible when approached from the remote bands side, producing sawtooth features in the inverse compressibility vs filling,  $\nu$ , plots [15, 19–21, 23]. This led the authors of Ref. [15] to propose a simple “Dirac revival” picture based on the strictly intermediate coupling of a simplified model in which the non-interacting Bistritzer-MacDonald (BM) [1] bands are sequentially filled. In this picture, starting from the CNP the BM bands are filled equally until a critical  $\nu$  after which one of the flavors is nearly fully populated, while the densities of the remaining flavors are reset to somewhat below the CNP. The key source of itineracy for such a proposal is the dispersion of the BM bands. Unfortunately, the BM bands also feature *two* Dirac nodes per spin and valley, doubling the Landau level degeneracy away from each integer  $\nu$  to 8, 6, 4, 2 sequence, and mak-

ing this proposal inconsistent with the observed 4, 3, 2, 1 sequence.

Here we show that the non-trivial narrow band topology/geometry [29, 33, 36, 37, 39], neglected in the simplified model of Ref. [15], combined with Coulomb interaction can drive the itineracy of the single particle charge excitations near the integer  $\nu$  even in strong coupling, i.e. when the BM kinetic energy is neglected. In addition to insulating phases belonging to spin-valley U(4) or U(4)×U(4) manifold [42, 55, 63], the interplay of band topology/geometry and strong Coulomb interactions was shown to make the strong coupling nematic phases, which are semi-metallic, energetically competitive [46, 58]. The nematic phase was recently shown to be further stabilized by strain [75]. Absence of gaps is therefore not at variance with the strong coupling picture.

Interestingly, in all of these phases, whether insulating or semi-metallic, the band minimum of the single particle charge excitations appears at  $\Gamma$ , the center of the moire Brillouin zone (mBZ), naturally producing the experimentally observed sequence of weak magnetic field Landau level degeneracies. Here we provide an explanation of this observation and find that the strong coupling band degeneracies are a consequence of a novel action of the combination of the unitary particle-hole [37] and the  $C_2\mathcal{T}$  symmetries. We find that the band dispersion of a single particle or a single hole added to the strong coupling phases at a non-zero integer  $\nu$  is highly asymmetric (see Fig. 1). If the excitation moves  $\nu$  closer to (away from) the CNP it is heavy with a narrow bandwidth (light with a large bandwidth). The light mass excitations have a minimum at  $\Gamma$  and a smaller degeneracy than the heavy ones, whose minima are away from a high symmetry  $\mathbf{k}$ -point. At a finite density away from an integer  $\nu$ , the single particle excitations repel each other [64]. By estimating the ratio of the residual interaction to the kinetic

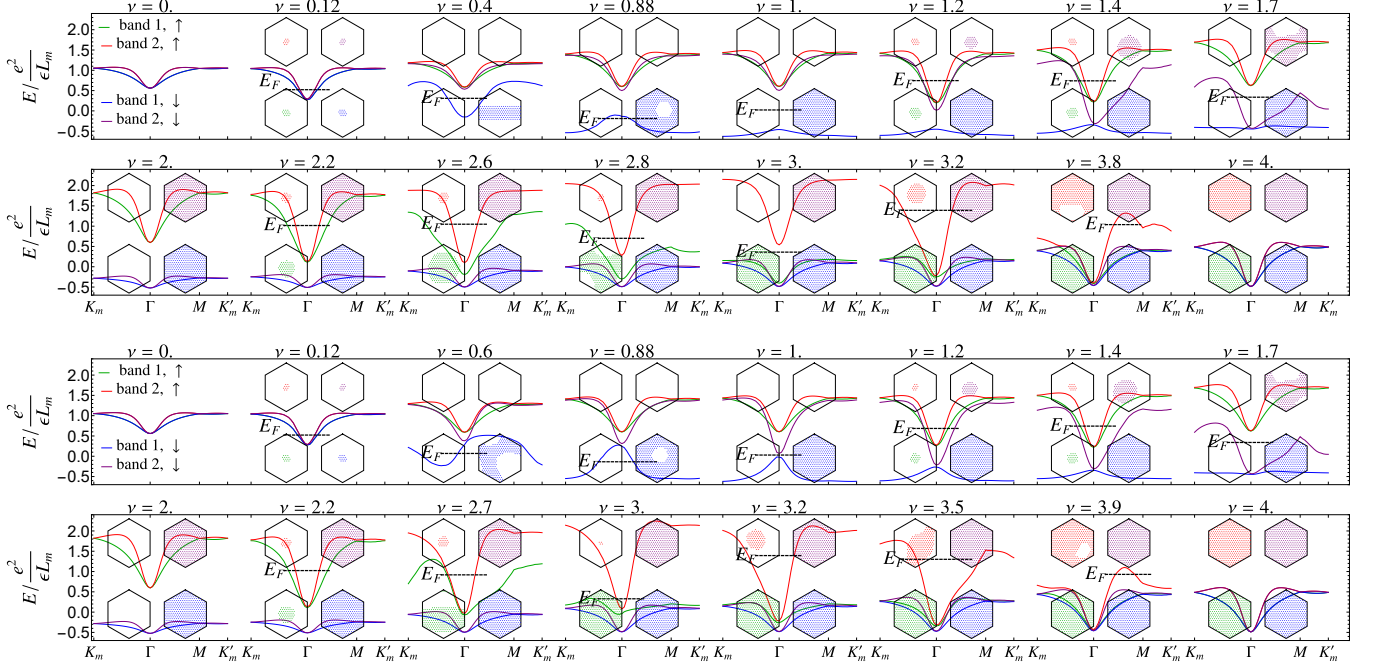


FIG. 1. Quasiparticle bands at different fillings  $\nu$  for the trial state  $|\Psi_{GS}\rangle$  at  $w_0/w_1 = 0.7$  when the  $C_2\mathcal{T}$  symmetry is allowed to be broken (top two panels) and when  $C_2\mathcal{T}$  is enforced (bottom two panels). The hexagonal insets show occupied  $\mathbf{k}$  points.

energy obtained by filling the new (non-rigid) bands, the system on the small mass side is a Fermi liquid. The mass compares favorably with experiments[79]. On the heavy mass side, we found several nearly degenerate states that are related by many particle-hole excitations, suggesting that there, the residual interactions lead to additional instabilities of a heavy Fermi liquid. This explains the

observed Landau fans pointing away from the CNP and their degeneracies. The chemical potential  $\mu$  is similar to experiments, including negative compressibilities and the overall magnitude of its difference between fully occupied and empty eight narrow bands, regardless of whether the strong coupling states at odd integer  $\nu$  are gapped or gapless (see Fig. 2).

Our starting Hamiltonian includes only the momentum conserving Coulomb interactions (renormalized by the remote bands) projected onto the BM narrow bands

$$H = \frac{1}{2A} \sum_{\mathbf{q} \neq 0} V(\mathbf{q}) \delta \rho_{\mathbf{q}} \delta \rho_{-\mathbf{q}}. \quad (1)$$

Here  $A$  is the area of the system,  $V(\mathbf{q}) = (\epsilon q / (2\pi e^2) + \Pi(\mathbf{q}))^{-1}$  [53], for the encapsulating hexagonal boron-nitride  $\epsilon = 4.4$ , and the static polarization function  $\Pi(\mathbf{q})$  originates from the remote bands [77–79].  $\delta \rho_{\mathbf{q}} = \rho_{\mathbf{q}} - \bar{\rho}_{\mathbf{q}}$  is the difference between the projected density operator and the background charge density, and  $\mathbf{q}$  is not restricted to the first mBZ (unlike the sum over  $\mathbf{k}$  below).

Specifically,

$$\rho_{\mathbf{q}} = \sum_{\substack{\tau=\mathbf{K}, \mathbf{K}' \\ s=\uparrow\downarrow}} \sum_{\substack{\mathbf{k} \in \text{mBZ} \\ n, n'=\pm}} \Lambda_{nn'}^{\tau}(\mathbf{k}, \mathbf{k} + \mathbf{q}) d_{\tau, n, s, \mathbf{k}}^{\dagger} d_{\tau, n', s, \mathbf{k} + \mathbf{q}} \quad (2)$$

$$\bar{\rho}_{\mathbf{q}} = 2 \sum_{\mathbf{G}, n=\pm} \delta_{\mathbf{q}, \mathbf{G}} \sum_{\mathbf{k} \in \text{mBZ}} \Lambda_{nn}^{\mathbf{K}}(\mathbf{k}, \mathbf{k} + \mathbf{G}), \quad (3)$$

where  $\rho_{\mathbf{q}}$  is expressed in the Chern basis  $\Phi_{\tau, \pm, \mathbf{k}}(\mathbf{r})$  that carries the indices of the valley  $\tau = \mathbf{K}$  or  $\mathbf{K}'$ , the Chern  $n = \pm$ , the spin  $s = \uparrow\downarrow$ , and the  $\mathbf{k}$ , for creation and annihilation operators  $d^{\dagger}$  and  $d$ . The Chern states are the sublattice polarized states of the BM model for narrow bands [55, 58] at the magic angle i.e.  $w_1/(v_F k_{\theta}) = 0.586$  and  $w_0/w_1 = 0.7$ , where  $w_0$  and  $w_1$  are the two interlayer couplings [28, 29, 41],  $v_F$  is the Fermi velocity for the monolayer graphene,  $k_{\theta} = 8\pi/(3L_m) \sin(\theta/2)$  and  $L_m$  is the moire lattice constant. Spinless time reversal symmetry relates the valleys  $\mathbf{K}$  and  $\mathbf{K}'$  [27–29]. The form factor matrix  $\Lambda_{mn}^{\tau}(\mathbf{k}, \mathbf{k} + \mathbf{q}) =$

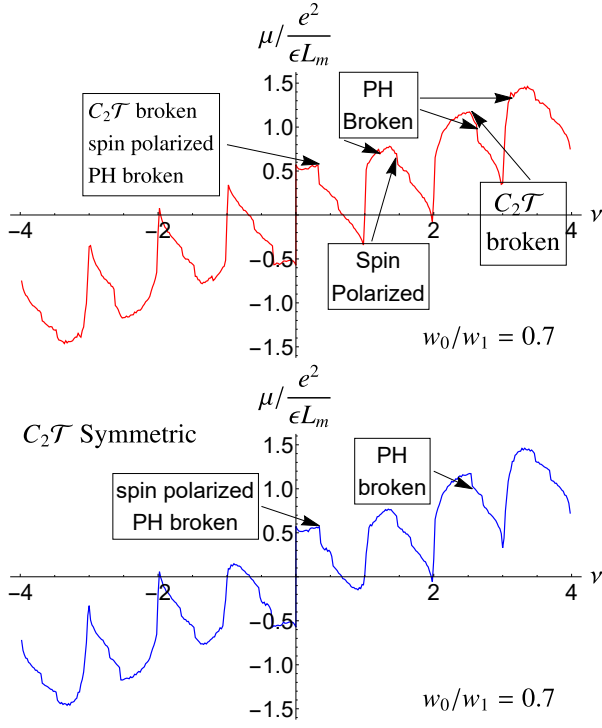


FIG. 2. Chemical potential  $\mu$  as the filling  $\nu$  varies between  $-4$  and  $4$  when  $C_2\mathcal{T}$  symmetry is allowed to be broken (top panel) and when  $C_2\mathcal{T}$  is enforced (bottom panel).

$\int_{uc} d\mathbf{r} e^{-i\mathbf{q}\cdot\mathbf{r}} \Phi_{\tau,m,\mathbf{k}}^*(\mathbf{r}) \Phi_{\tau,n,\mathbf{k}+\mathbf{q}}(\mathbf{r})$  contains the information about the non-trivial topology/geometry of the narrow bands and plays an important role in the physics we describe; it has been neglected in Ref. [15].

Previous analytical and numerical works showed that over a large range of parameters the ground states  $|\Psi_{GS}\rangle$  of  $H$  in (1) are Slater determinants [42, 55, 58, 63, 65]. At even integer  $\nu$  they consist of all states that satisfy [55, 59, 63]

$$\delta\rho_{\mathbf{q}}|\Psi_{GS}\rangle = \frac{\nu}{4} \sum_{\mathbf{G}} \delta_{\mathbf{q},\mathbf{G}} \bar{\rho}_{\mathbf{G}} |\Psi_{GS}\rangle, \quad (4)$$

with the eigenenergy  $E_{\nu} = \frac{1}{2A} \sum_{\mathbf{G} \neq 0} V(\mathbf{G}) \left| \frac{\nu}{4} \bar{\rho}_{\mathbf{G}} \right|^2$ . The exact excited states can also be obtained [59, 64]. Indeed, acting with  $H$  on the state  $\hat{X}|\Psi_{GS}\rangle$ , where  $\hat{X}$  is some combination of  $d^\dagger$ 's and  $d$ 's, and using (4)

$$(H - E_{\nu})\hat{X}|\Psi_{GS}\rangle = \frac{1}{2A} \sum_{\mathbf{q}} V(\mathbf{q}) \left( [\delta\rho_{-\mathbf{q}}, [\delta\rho_{\mathbf{q}}, \hat{X}]] + [\delta\rho_{\mathbf{q}}, \hat{X}]\delta\rho_{-\mathbf{q}} + [\delta\rho_{-\mathbf{q}}, \hat{X}]\delta\rho_{\mathbf{q}} \right) |\Psi_{GS}\rangle. \quad (5)$$

The last two terms can be further simplified by applying (4). Because each commutator has the same number of  $d^\dagger$ 's and  $d$ 's as the ones in  $\hat{X}$ , we can match the coefficients. This was used to find the charge neutral collective modes [59, 64] and to show that the spectrum of charge-2 elementary excitations for a purely repulsive

$V(\mathbf{q})$  does not have a bound state [64]. For  $\hat{X}_+ = d_{\tau,n,s,\mathbf{k}}^\dagger$  and  $\hat{X}_- = d_{\tau,n,s,\mathbf{k}}$ , Eqn.(5) reduces to solving for eigenvalues of the  $2 \times 2$  matrix

$$\mathcal{E}_{n'n,\pm}^{\tau}(\mathbf{k}) = \frac{1}{2A} \left( \sum_{\mathbf{q}} V(\mathbf{q}) \sum_m \Lambda_{mn}^{\tau}(\mathbf{k} - \mathbf{q}, \mathbf{k}) \Lambda_{n'm}^{\tau}(\mathbf{k}, \mathbf{k} - \mathbf{q}) \pm \frac{\nu}{2} \sum_{\mathbf{G}} V(\mathbf{G}) \bar{\rho}_{\mathbf{G}} \Lambda_{n'n}^{\tau}(\mathbf{k} + \mathbf{G}, \mathbf{k}) \right), \quad (6)$$

that leads to 2 different bands for both electron and hole excitations for each spin  $s$ . To illustrate the main effect, consider first the chiral limit [41, 80, 81],  $w_0/w_1 = 0$  when the Chern states are perfectly sublattice polarized. Therefore,  $\Lambda_{mn}^{\tau}(\mathbf{k}, \mathbf{k} + \mathbf{q})$  is diagonal in  $m, n$  and Slater determinant states obtained by filling Chern bands satisfy (4) also at odd filling; they have been shown to be the ground states in exact diagonalization (ED) studies in Ref. [65]. The spectrum of the single particle excitations can then be solved using (6) at any integer filling. The eigenstates of  $\mathcal{E}_{n'n,+}^{\tau}(\mathbf{k})$  are exactly degenerate over the whole mBZ, as are the eigenstates of  $\mathcal{E}_{n'n,-}^{\tau}(\mathbf{k})$ . This is due to the combination of the 2-fold rotation about the axis normal to the plane, spinless time reversal and the chiral particle-hole symmetries [41, 55, 60, 62],  $\mathcal{K}' = C_2\mathcal{T}\mathcal{C}$ . Because  $\mathcal{K}'$  preserves  $\mathbf{k}$  and  $\mathcal{K}'^2 = -1$ ,  $\mathcal{E}_{n'n,\pm}^{\tau}(\mathbf{k})$  must be proportional to  $\delta_{mn}$  for each  $\mathbf{k}$ .

For  $w_0/w_1 \neq 0$  the particle and hole dispersions are the same at the CNP. The two bands are now degenerate only at high symmetry points  $\Gamma$ ,  $\mathbf{M}$ ,  $\mathbf{K}_m$  and  $\mathbf{K}'_m$  (see Fig. 1). The degeneracies at  $\Gamma$  and  $\mathbf{M}$  are protected by  $C_2\mathcal{T}$  times particle-hole symmetry  $\mathcal{P}$  discussed in Refs. [37, 59, 79]. Combined with  $C_3$  symmetry, the winding numbers at  $\Gamma$  and  $\mathbf{M}$  can be shown to be 3 and  $-1$  respectively. The degeneracy at  $\mathbf{K}_m$  (and  $\mathbf{K}'_m$ ) is protected by  $C_3$  with the winding number of 1 (see [79]).

Although such degeneracy is also seen at  $\nu = \pm 2, \pm 4$ , excitation spectra are markedly different. The bands away from CNP have the minimum at  $\Gamma$  and wide bandwidth. However, the bands towards CNP are narrower with minima away from high symmetry  $\mathbf{k}$  points. To understand this, we return to the chiral limit ( $w_0/w_1 = 0$ ) with two gate screened Coulomb interaction (with the distance to the metallic gate  $\xi = 5L_m$ ) and analyze the first (exchange) and the second (direct) terms in (6). Both terms can be well approximated by a nearest neighbor (NN) tight-binding model on a triangular lattice [79, 82, 83] with NN hopping amplitudes  $t_E = -0.0530 \frac{e^2}{\epsilon L_m}$  and  $t_D = -0.0523 \frac{e^2}{\epsilon L_m}$ , and with onsite terms  $\epsilon_E = 1.714 \frac{e^2}{\epsilon L_m}$  and  $\epsilon_D = 0.333 \frac{e^2}{\epsilon L_m}$  for exchange and direct terms respectively [79, 82]. This, as well as our  $\mathbf{k} \cdot \mathbf{p}$  analysis around the  $\mathbf{K}_m$  point based on Ref. [61, 79], show that the minimum of the dispersion is at  $\Gamma$  when the two terms add. When they subtract, the bandwidth is reduced. The magnitudes of the NN hoppings  $t_E$  and  $t_D$  are such that at  $\nu = \pm 1$  the cancellation is nearly

complete, leading to the narrow band of heavy holes at  $\nu = 1$  and heavy particles at  $\nu = -1$ . For  $|\nu| \geq 2$ , the dispersions towards CNP reverse compared to  $\nu = 0$ , also with heavy excitations. Because for excitations at  $\nu \neq 0$  that are moving the filling away from the CNP the direct and the exchange terms add (in absolute value), the resulting bands are more dispersive with a minimum at  $\Gamma$ . These are the light fermions. As seen in Fig.1, the effect persists away from the chiral limit  $w_0/w_1 \neq 0$ .

At a finite density away from an integer  $\nu$  the excitations mutually interact[59, 64] as seen from (5). Nevertheless, the steep dispersion of a *single* electron (hole) added to the exact eigenstates at the positive (negative) integer  $\nu$  and at CNP suggests that at a finite density close to the integer  $\nu$  – and in the direction away from CNP – the kinetic energy of such excitations is sufficient to stabilize a Fermi liquid. This is broadly consistent with the ED results of Ref. [84], where emergent Fermi liquids were also found in different, albeit related, models of moire heterostructures. We therefore approximate the ground state by the trial state  $|\Psi_{GS}\rangle = \prod_{s,\mathbf{k}} \hat{P}_{s,\mathbf{k}} |\Psi_{CNP}\rangle$  where  $|\Psi_{CNP}\rangle$  is a ground state at CNP which, without loss of generality, is taken to be completely  $\mathbf{K}'$  valley polarized with all four  $\mathbf{K}$  bands empty. At each  $s, \mathbf{k}$  there are two bands at  $\mathbf{K}$  whose occupation is determined by  $\nu_{s,\mathbf{k}}$ ; when empty ( $\nu_{s,\mathbf{k}} = 0$ )  $\hat{P}_{s,\mathbf{k}} = 1$  and when doubly occupied ( $\nu_{s,\mathbf{k}} = 2$ )  $\hat{P}_{s,\mathbf{k}} = d_{\mathbf{K},+,s,\mathbf{k}}^\dagger d_{\mathbf{K},-,s,\mathbf{k}}^\dagger$ . When singly occupied ( $\nu_{s,\mathbf{k}} = 1$ ), we have  $\hat{P}_{s,\mathbf{k}} = u_{s,\mathbf{k}} d_{\mathbf{K},+,s,\mathbf{k}}^\dagger + v_{s,\mathbf{k}} d_{\mathbf{K},-,s,\mathbf{k}}^\dagger$  with variational parameters satisfying  $|u_{s,\mathbf{k}}|^2 + |v_{s,\mathbf{k}}|^2 = 1$ . The integer parameters  $\nu_{s,\mathbf{k}}$  are also determined variationally and satisfy the constraint  $\sum_{s,\mathbf{k}} \nu_{s,\mathbf{k}} = \nu N_{uc}$ , where  $N_{uc}$  is the total number of moire unit cells. Minimizing  $E = \langle \Psi_{GS} | H | \Psi_{GS} \rangle$  subject to the mentioned constraints yields the self-consistent eigen-equations for  $u_{s,\mathbf{k}}$  and  $v_{s,\mathbf{k}}$

$$H_{eff}(s, \mathbf{k}) \begin{pmatrix} u_{s,\mathbf{k}} \\ v_{s,\mathbf{k}} \end{pmatrix} = E_\alpha(s, \mathbf{k}) \begin{pmatrix} u_{s,\mathbf{k}} \\ v_{s,\mathbf{k}} \end{pmatrix}. \quad (7)$$

$H_{eff}$  is detailed in SM [79].  $E_\alpha(s, \mathbf{k})$  specifies the band structure shown in Fig. 1. Fig. 2 shows the  $\nu$  dependence of chemical potential  $\mu$ , calculated from the constraint  $\sum_{\alpha,s,\mathbf{k}} \Theta(\mu - E_\alpha(s, \mathbf{k})) = \nu N_{uc}$ . The following discussion focuses on  $\nu \geq 0$ , the states with  $\nu < 0$  can be obtained using the many-body particle-hole symmetry [62].

At  $\nu = 2$ , our variational method results in  $|\Psi_{GS}^{\nu=2}\rangle = \prod_{n=\pm,\mathbf{k}} d_{\mathbf{K},n,s,\mathbf{k}}^\dagger |\Psi_{CNP}\rangle$  where the spin  $s = \uparrow$  or  $\downarrow$ . Although this exact (gapped) eigen-state breaks the time reversal symmetry (spinfull and spinless), it does not break  $C_2\mathcal{T}$ . Thus it carries zero Chern number. It was also numerically shown to be the ground state [65]. Its single particle excitation spectrum produced by (7) is the same as the ones obtained in (6). At odd integer  $\nu$  with  $w_0/w_1 = 0.7$  this method results in the quantum anomalous Hall (QAH) state with spontaneously broken  $C_2\mathcal{T}$  symmetry if no additional constraints are applied

as shown in the upper two panels of Fig. 1. This result is consistent with the exact solution obtained in the chiral limit ( $w_0/w_1 = 0$ ), the recent DMRG calculation [58, 70] and the ED [65] for a range of  $w_0/w_1 \neq 0$ . For comparison, applying the  $C_2\mathcal{T}$  symmetric constraint to the odd  $\nu$  trial state  $|\Psi_{GS}\rangle$  leads to a semi-metallic state as shown in the lower two panels of Fig. 1. Both the  $C_2\mathcal{T}$  broken Chern insulators and  $C_2\mathcal{T}$  symmetric gapless states are nearly degenerate, as also demonstrated by DMRG and ED calculations [58, 65, 70].

At non-integer fillings  $|\Psi_{GS}\rangle$  leads to gapless compressible phases. The details of the band evolution with  $\nu$  are shown in Fig. 1. At  $\nu$  just above the positive integers the gapless excitation spectrum is strongly dispersive, with the bandwidth set by  $e^2/(\epsilon L_m)$ . As discussed below, we expect such low compressibility phases to be stable when the residual interaction that scatters among different trial states is included, resulting in Fermi liquids at these fillings. Furthermore, the cyclotron mass is roughly proportional to the difference between  $\nu$  and the integer [79]. The ultimate instability of the Fermi liquids upon approaching a positive integer  $\nu$  from below stems from the mentioned residual interactions *and* the fact that the band structure is not rigid, with the partially filled band(s) flattening as  $\nu$  approaches an integer (see Fig. 1). Even within this simple variational method, which does not account for the residual interactions, there are several Stoner-like phase transitions as the integer  $\nu$  is approached from below. Such spontaneous breaking of  $C_2\mathcal{T}$ , particle-hole, or  $C_3$  symmetries, furthers the instabilities of the Fermi liquid. We found the transition occurring between  $\nu = 0$  and  $\nu = 1$  to be first order, becoming a second order between higher integers fillings.

As illustrated in Fig. 2, at each non-negative integer  $\nu$ , the chemical potential  $\mu$  increases as  $\nu$  moves away from the CNP. Before  $\nu$  gets to the next integer,  $\mu$  reaches its local maximum at a fractional filling and then decreases, resulting in the negative compressibility  $\frac{d\mu}{d\nu}$ . The net increase of  $\mu$  is  $\sim 40\text{meV}$  which compares well with  $\sim 50\text{meV}$  found in experiments [10, 14, 15, 19, 23].

Because the dominant residual interaction is repulsive [59, 64], we estimate its importance over dispersion in two different ways. *First*, we consider  $r_s$ , defined as the ratio of  $U(\bar{r}) = \int \frac{d^2\mathbf{q}}{(2\pi)^2} V(q) e^{i\mathbf{q}\cdot\bar{\mathbf{r}}}$ , i.e. the residual Coulomb potential energy of two excitations separated by  $\bar{r} = 1/\sqrt{\delta n}$ , and the average kinetic energy  $E_K$ ; here  $\delta n$  is the density deviation from the closest integer filling. For an electron excitation of a partially filled band we define  $E_K^e = \int_{filled} \frac{d^2\mathbf{k}}{(2\pi)^2} (E(\mathbf{k}) - E_{\min})$  where  $E_{\min}$  is the band minimum, while for hole excitations,  $E_K^h = \int_{unfilled} \frac{d^2\mathbf{k}}{(2\pi)^2} (E_{\max} - E(\mathbf{k}))$  where  $E_{\max}$  is the band maximum. Then,  $E_K$  is set to be the smaller of  $E_K^e$  and  $E_K^h$ . As  $\nu$  approaches an integer,  $\delta n \rightarrow 0$  and  $r_s = U(\bar{r})/E_K$  diverges because  $U(\bar{r}) \sim O(\sqrt{\delta n})$  and

$E_K \sim O(\delta n)$ . For  $m < \nu \lesssim m + 0.017$  where  $m$  is a non-negative integer, we find  $r_s \geq 35$ , i.e.  $r_s$  is above the critical value for the Wigner crystallization [85, 86]. If we include additional screening due to the nearby metallic gates,  $U(r)$  is modified from  $1/r$  at long distances and decays faster when  $r$  is larger than the distance to gates  $l_g$ . Therefore  $U(\bar{r}) \ll E_K$  at small  $\delta n$ , eliminating a possible Wigner crystal if  $\delta n < l_g^{-2}$ . For a typical gate distance  $l_g \sim 40\text{nm}$ , the screened Coulomb interaction eliminates the Wigner crystal if  $m < \nu \lesssim m + 0.09$ . Therefore, no Wigner crystal should exist close to an integer filling on the side away from the CNP.

*Second*, we calculate the ratio between  $U(\bar{r})$  and  $W$ , the bandwidth of the excitations. If  $m < \nu \lesssim m + 0.3$ , then  $U(\bar{r})/W \lesssim 0.3$ , suggesting that the system is in the weak coupling regime. Together with the above analysis of  $r_s$ , we conclude that the system is in the Fermi liquid phase if the filling is in this interval. Moreover, as illustrated in Fig. 1, in this filling interval the  $4 - m$  partially occupied bands are filled equally near  $\Gamma$ , resulting in the experimentally observed Landau fan degeneracy of  $4 - m$  when pointing away from the CNP [2–4, 8].

On the other hand, for  $m + 0.4 \lesssim \nu < m + 1$ , the variational calculation resulted in the band reconstruction and several nearly degenerate states. These states are related by many particle-hole excitations, implying that the obtained states are likely unstable upon including the residual interactions between the quasi-particles. These bands are narrow at every integer filling for excitations towards the CNP, naturally explaining the absence of the Landau fans towards the CNP [2–4, 8].

The framework presented here provides a strong coupling description of the itinerant carriers, whose residual interactions *and* dispersion both depend on the Coulomb interaction. The description of the charge itineracy presented here is in quantitative agreement with experiments, and builds a framework within which superconductivity, emerging at lower temperatures at some fillings, should be understood.

J. K. acknowledges the support from the NSFC Grant No. 12074276, and the Priority Academic Program Development (PAPD) of Jiangsu Higher Education Institutions. B. A. B. is supported by the ONR No. N00014-20-1-2303 and partially by DOE Grant No. DE-SC0016239, NSF- MRSEC No. DMR-1420541 and DMR-2011750. O. V. is supported by NSF DMR-1916958 and partially by the National High Magnetic Field Laboratory through NSF Grant No. DMR-1157490 and the State of Florida. This research was facilitated by the KITP program “Correlated Systems with Multicomponent Local Hilbert Spaces”, supported in part by the National Science Foundation under Grant No. NSF PHY-1748958.

\* jkang@suda.edu.cn

† vafek@magnet.fsu.edu

- [1] R. Bistritzer and A. H. MacDonald, “Moire bands in twisted double-layer graphene,” Proc. Natl. Acad. Sci. U.S.A. **108**, 12233 (2011).
- [2] Y. Cao, V. Fatemi, A. Demir, S. Fang, S. L. Tomarken, J. Y. Luo, J. D. Sanchez-Yamagishi, K. Watanabe, T. Taniguchi, E. Kaxiras, R. C. Ashoori, and P. Jarillo-Herrero, “Correlated insulator behaviour at half-filling in magic-angle graphene superlattices,” Nature **556**, 43 (2018).
- [3] Y. Cao, V. Fatemi, S. Fang, K. Watanabe, T. Taniguchi, E. Kaxiras, and P. Jarillo-Herrero, “Unconventional superconductivity in magic-angle graphene superlattices,” Nature **556**, 80 (2018).
- [4] M. Yankowitz, S. Chen, H. Polshyn, Y. Zhang, K. Watanabe, T. Taniguchi, D. Graf, A. F. Young, and C. R. Dean, “Tuning superconductivity in twisted bilayer graphene,” Science **363**, 1059 (2019).
- [5] A. L. Sharpe, E. J. Fox, A. W. Barnard, J. Finney, K. Watanabe, T. Taniguchi, M. A. Kastner, and D. Goldhaber-Gordon, “Emergent ferromagnetism near three-quarters filling in twisted bilayer graphene,” Science **365**, 605 (2019).
- [6] M. Serlin, C. L. Tschirhart, H. Polshyn, Y. Zhang, J. Zhu, K. Watanabe, T. Taniguchi, L. Balents, and A. F. Young, “Intrinsic quantized anomalous hall effect in a moire heterostructure,” Science science.aay5533 (2019).
- [7] A. Kerelsky, L. J. McGilly, D. M. Kennes, L. Xian, M. Yankowitz, S. Chen, K. Watanabe, T. Taniguchi, J. Hone, C. Dean, A. Rubio, and A. N. Pasupathy, “Maximized electron interactions at the magic angle in twisted bilayer graphene,” Nature **572**, 95 (2019).
- [8] X. Lu, P. Stepanov, W. Yang, M. Xie, M. A. Aamir, I. Das, C. Urgell, K. Watanabe, T. Taniguchi, G. Zhang, A. Bachtold, A. H. MacDonald, and D. K. Efetov, “Superconductors, orbital magnets and correlated states in magic-angle bilayer graphene,” Nature **574**, 653 (2019).
- [9] Y. Xie, B. Lian, B. Jack, X. Liu, C.-L. Chiu, K. Watanabe, T. Taniguchi, B. A. Bernevig, and A. Yazdani, “Spectroscopic signatures of many body correlations in magic-angle twisted bilayer graphene,” Nature **572**, 101 (2019).
- [10] S. L. Tomarken, Y. Cao, A. Demir, K. Watanabe, T. Taniguchi, P. Jarillo-Herrero, and R. C. Ashoori, “Electronic compressibility of magic-angle graphene superlattices,” Phys. Rev. Lett. **123**, 046601 (2019).
- [11] Y. Jiang, X. Lai, K. Watanabe, T. Taniguchi, K. Haule, J. Mao, and E. Y. Andrei, “Charge order and broken rotational symmetry in magic-angle twisted bilayer graphene,” Nature **573**, 91 (2019).
- [12] Y. Choi, J. Kemmer, Y. Peng, A. Thomson, H. Arora, R. Polski, Y. Zhang, H. Ren, J. Alicea, G. Refael, F. von Oppen, K. Watanabe, T. Taniguchi, and S. Nadj-Perge, “Electronic correlations in twisted bilayer graphene near the magic angle”, Nat. Phys. **15**, 1174 (2019).
- [13] P. Stepanov, I. Das, X. Lu, A. Fahimniya, K. Watanabe, T. Taniguchi, F. H. L. Koppens, J. Lischner, L. Levitov, D. K. Efetov, “Untying the insulating and superconducting orders in magic-angle graphene”, Nature **583**, 375 (2020).

- [14] D. Wong, K. P. Nuckolls, M. Oh, B. Lian, Y. Xie, S. Jeon, K. Watanabe, T. Taniguchi, B. A. Bernevig, and A. Yazdani, “Cascade of electronic transitions in magic-angle twisted bilayer graphene,” *Nature* **582**, 198 (2020).
- [15] U. Zondiner, A. Rozen, D. Rodan-Legrain, Y. Cao, R. Queiroz, T. Taniguchi, K. Watanabe, Y. Oreg, F. von Oppen, A. Stern, E. Berg, P. Jarillo-Herrero, and S. Ilani, “Cascade of Phase Transitions and Dirac Revivals in Magic Angle Graphene,” *Nature* **582**, 203 (2020).
- [16] Y. Saito, J. Ge, K. Watanabe, T. Taniguchi, and A. F. Young, “Independent superconductors and correlated insulators in twisted bilayer graphene,” *Nat. Phys.* **16**, 926 (2020).
- [17] Y. Cao, D. Rodan-Legrain, J. M. Park, F. N. Yuan, K. Watanabe, T. Taniguchi, R. M. Fernandes, L. Fu, and P. Jarillo-Herrero, “Nematicity and Competing Orders in Superconducting Magic-Angle Graphene,” arXiv:2004.04148.
- [18] C. L. Tschirhart, M. Serlin, H. Polshyn, A. Shragai, Z. Xia, J. Zhu, Y. Zhang, K. Watanabe, T. Taniguchi, M. E. Huber, A. F. Young, “Imaging orbital ferromagnetism in a moire Chern insulator”, arXiv:2006.08053.
- [19] Y. Saito, F. Yang, J. Ge, X. Liu, K. Watanabe, T. Taniguchi, J.I.A. Li, E. Berg, and A. F. Young, “Isospin Pomeranchuk effect and the entropy of collective excitations in twisted bilayer graphene”, arXiv:2008.10830.
- [20] A. Rozen, J. M. Park, U. Zondiner, Y. Cao, D. Rodan-Legrain, T. Taniguchi, K. Watanabe, Y. Oreg, A. Stern, E. Berg, P. Jarillo-Herrero, and S. Ilani, “Entropic evidence for a Pomeranchuk effect in magic angle graphene”, arXiv:2009.01836.
- [21] Y. Choi, H. Kim, Y. Peng, A. Thomson, C. Lewandowski, R. Polski, Y. Zhang, H. S. Arora, K. Watanabe, T. Taniguchi, J. Alicea, and S. Nadj-Perge, “Correlation-driven topological phases in magic-angle twisted bilayer graphene”, *Nature* **589**, 536 (2021).
- [22] Y. Saito, J. Ge, L. Rademaker, K. Watanabe, T. Taniguchi, D. A. Abanin, and A. F. Young, “Hofstadter subband ferromagnetism and symmetry broken Chern insulators in twisted bilayer graphene”, *Nat. Phys.* (2021).
- [23] A. T. Pierce, Y. Xie, J. M. Park, E. Khalaf, S. H. Lee, Y. Cao, D. E. Parker, P. R. Forrester, S. Chen, K. Watanabe, T. Taniguchi, A. Vishwanath, P. Jarillo-Herrero, and A. Yacoby, “Unconventional sequence of correlated Chern insulators in magic-angle twisted bilayer graphene”, arXiv:2101.04123.
- [24] X. Liu, Z. Wang, K. Watanabe, T. Taniguchi, O. Vafek, and J.I.A. Li, “Tuning electron correlation in magic-angle twisted bilayer graphene using Coulomb screening”, *Science*, science.abb8754 (2021).
- [25] S. Wu, Z. Zhang, K. Watanabe, T. Taniguchi and E. Y. Andrei, “Chern insulators, van Hove singularities and topological flat bands in magic-angle twisted bilayer graphene”, *Nature Materials* **20**, 488 (2021).
- [26] J. M. Park, Y. Cao, K. Watanabe, T. Taniguchi, and P. Jarillo-Herrero, “Flavour Hund’s coupling, Chern gaps and charge diffusivity in moiré graphene”, *Nature* **592**, 43 (2021).
- [27] J. Kang and O. Vafek, “Symmetry, maximally localized Wannier states, and a low-energy model for twisted bilayer graphene narrow bands,” *Phys. Rev. X* **8**, 031088 (2018).
- [28] M. Koshino, N. F. Q. Yuan, T. Koretsune, M. Ochi, K. Kuroki, and L. Fu, “Maximally localized wannier orbitals and the extended hubbard model for twisted bilayer graphene,” *Phys. Rev. X* **8**, 031087 (2018).
- [29] H. C. Po, L. Zou, A. Vishwanath, and T. Senthil, “Origin of mott insulating behavior and superconductivity in twisted bilayer graphene,” *Phys. Rev. X* **8**, 031089 (2018).
- [30] F. Wu, A. H. MacDonald, and I. Martin, “Theory of phonon-mediated superconductivity in twisted bilayer graphene,” *Phys. Rev. Lett.* **121**, 257001 (2018).
- [31] H. Isobe, N. F. Q. Yuan, and L. Fu, “Unconventional superconductivity and density waves in twisted bilayer graphene,” *Phys. Rev. X* **8**, 041041 (2018).
- [32] F. Guinea and N. R. Walet, “Electrostatic effects, band distortions, and superconductivity in twisted graphene bilayers,” *Proc. Natl. Acad. Sci. U.S.A.* **115**, 13174 (2018).
- [33] L. Zou, H. C. Po, A. Vishwanath, and T. Senthil, “Band structure of twisted bilayer graphene: Emergent symmetries, commensurate approximants, and Wannier obstructions,” *Phys. Rev. B* **98**, 085435 (2018).
- [34] M. Ochi, M. Koshino, K. Kuroki, “Possible correlated insulating states in magic-angle twisted bilayer graphene under strongly competing interactions”, *Phys. Rev. B* **98**, 081102 (2018).
- [35] L. Balents, “General continuum model for twisted bilayer graphene and arbitrary smooth deformations”, *SciPost Phys.*, **7**, 48 (2019).
- [36] J. Ahn, S. Park, and B.-J. Yang, “Failure of nielsen-nomiya theorem and fragile topology in two dimensional systems with space-time inversion symmetry: Application to twisted bilayer graphene at magic angle,” *Phys. Rev. X* **9**, 021013 (2019).
- [37] Z. Song, Z. Wang, W. Shi, G. Li, C. Fang, and B. Andrei Bernevig, “All magic angles in twisted bilayer graphene are topological,” *Phys. Rev. Lett.* **123**, 036401 (2019).
- [38] K. Hejazi, C. Liu, H. Shapourian, X. Chen, and L. Balents, “Multiple topological transitions in twisted bilayer graphene near the first magic angle,” *Phys. Rev. B* **99**, 035111 (2019).
- [39] J. Liu, J. Liu, and X. Dai, “The pseudo-Landau-level representation of twisted bilayer graphene: band topology and the implications on the correlated insulating phase,” *Phys. Rev. B* **99**, 155415 (2019).
- [40] J. Gonzalez and T. Stauber, “Kohn-luttinger superconductivity in twisted bilayer graphene,” *Phys. Rev. Lett.* **122**, 026801 (2019).
- [41] G. Tarnopolsky, A. J. Kruchkov, and A. Vishwanath, “Origin of magic angles in twisted bilayer graphene,” *Phys. Rev. Lett.* **122**, 106405 (2019).
- [42] J. Kang and O. Vafek, “Strong coupling phases of partially filled twisted bilayer graphene narrow bands,” *Phys. Rev. Lett.* **122**, 246401 (2019).
- [43] K. Seo, V. N. Kotov, and B. Uchoa, “Ferromagnetic Mott state in twisted graphene bilayers at the magic angle,” *Phys. Rev. Lett.* **122**, 246402 (2019).
- [44] Y.-H. Zhang, D. Mao, Y. Cao, P. Jarillo-Herrero, and T. Senthil, “Nearly flat chern bands in moire superlattices,” *Phys. Rev. B* **99**, 075127 (2019).
- [45] Y. H. Zhang, H. C. Po, and T. Senthil, “Landau level degeneracy in twisted bilayer graphene: Role of symmetry breaking” *Phys. Rev. B* **100**, 125104 (2019).
- [46] S. Liu, E. Khalaf, J. Y. Lee, and A. Vishwanath, “Nematic topological semimetal and insulator in magic angle bilayer graphene at charge neutrality,” *Phys. Rev. Re-*



- search **3**, 013033 (2021).
- [47] Y. Alavirad and J. D. Sau, “Ferromagnetism and its stability from the one-magnon spectrum in twisted bilayer graphene,” *Phys. Rev. B* **102**, 235123 (2020).
- [48] J. Liu and X. Dai, “Correlated insulating states and the quantum anomalous Hall phenomena at all integer fillings in twisted bilayer graphene”, *Phys. Rev. B* **103**, 035427 (2021).
- [49] F. Wu and S. Das Sarma, “Collective Excitations of Quantum Anomalous Hall Ferromagnets in Twisted Bilayer Graphene”, *Phys. Rev. Lett.* **124**, 046403 (2020).
- [50] M. Xie, and A. H. MacDonald, “Nature of the Correlated Insulator States in Twisted Bilayer Graphene,” *Phys. Rev. Lett.* **124**, 097601 (2020).
- [51] N. Bultinck, S. Chatterjee, and M. P. Zaletel, “Mechanism for Anomalous Hall Ferromagnetism in Twisted Bilayer Graphene,” *Phys. Rev. Lett.* **124**, 166601 (2020).
- [52] C. Repellin, Z. Dong, Y.-H. Zhang, T. Senthil, “Ferromagnetism in narrow bands of moire superlattices,” *Phys. Rev. Lett.* **124**, 187601 (2020).
- [53] T. Cea and F. Guinea, “Band structure and insulating states driven by Coulomb interaction in twisted bilayer graphene”, *Phys. Rev. B* **102**, 045107 (2020).
- [54] S. Chatterjee, N. Bultinck, and M. P. Zaletel, “Symmetry breaking and skyrmionic transport in twisted bilayer graphene,” *Phys. Rev. B* **101**, 165141 (2020).
- [55] N. Bultinck, E. Khalaf, S. Liu, S. Chatterjee, A. Vishwanath, and M. P. Zaletel, “Ground State and Hidden Symmetry of Magic Angle Graphene at Even Integer Filling,” *Phys. Rev. X* **10**, 031034 (2020).
- [56] D. V. Chichinadze, L. Classen, and A. V. Chubukov, “Nematic superconductivity in twisted bilayer graphene,” *Phys. Rev. B* **101**, 224513 (2020).
- [57] Y. Zhang, K. Jiang, Z. Wang, and F. C. Zhang, “Correlated insulating phases of twisted bilayer graphene at commensurate filling fractions: a Hartree-Fock study,” *Phys. Rev. B* **102**, 035136 (2020).
- [58] J. Kang and O. Vafek, “Non-Abelian Dirac node braiding and near-degeneracy of correlated phases at odd integer filling in magic angle twisted bilayer graphene”, *Phys. Rev. B* **102**, 035161 (2020).
- [59] O. Vafek and J. Kang, “Renormalization Group Study of Hidden Symmetry in Twisted Bilayer Graphene with Coulomb Interactions,” *Phys. Rev. Lett.* **125**, 257602 (2020).
- [60] J. Wang, Y. Zheng, A. J. Millis, and J. Cano, “Chiral Approximation to Twisted Bilayer Graphene: Exact Intra-Valley Inversion Symmetry, Nodal Structure and Implications for Higher Magic Angles”, *arXiv:2010.03589*.
- [61] B. A. Bernevig, Z.-D. Song, N. Regnault, and B. Lian, “TBG I: Matrix Elements, Approximations, Perturbation Theory and a  $\mathbf{k}\cdot\mathbf{p}$  2-Band Model for Twisted Bilayer Graphene”, *arXiv:2009.11301*.
- [62] B. A. Bernevig, Z.-D. Song, N. Regnault, and B. Lian “TBG III: Interacting Hamiltonian and Exact Symmetries of Twisted Bilayer Graphene”, *arXiv:2009.12376*.
- [63] B. Lian, Z.-D. Song, N. Regnault, D. K. Efetov, A. Yazdani, and B. A. Bernevig, “TBG IV: Exact Insulator Ground States and Phase Diagram of Twisted Bilayer Graphene”, *arXiv:2009.13530*.
- [64] B. A. Bernevig, B. Lian, A. Cowsik, F. Xie, N. Regnault, Z.-D. Song, “TBG V: Exact Analytic Many-Body Excitations In Twisted Bilayer Graphene Coulomb Hamiltonians: Charge Gap, Goldstone Modes and Absence of Cooper Pairing,” *arXiv:2009.14200*.
- [65] F. Xie, A. Cowsik, Z.-D. Song, B. Lian, and B. A. Bernevig, and N. Regnault, “TBG VI: An Exact Diagonalization Study of Twisted Bilayer Graphene at Non-Zero Integer Fillings”, *arXiv:2010.00588*.
- [66] Y. D. Liao, J. Kang, C. N. Breio, X. Y. Xu, H.-Q. Wu, B. M. Andersen, R. M. Fernandes, and Z. Y. Meng, “Correlation-induced insulating topological phases at charge neutrality in twisted bilayer graphene”, *Phys. Rev. X* **11**, 011014 (2021).
- [67] R. M. Fernandes and J. W. F. Venderbos, “Nematicity with a twist: rotational symmetry breaking in a moire superlattice,” *Science Advances* **6**, eaba8834 (2020).
- [68] L. Balents, C. R. Dean, D. K. Efetov, and A. F. Young, “Superconductivity and strong correlations in moiré flat bands”, *Nat. Phys.* **16**, 725 (2020).
- [69] E. Brillaux, D. Carpentier, A. A. Fedorenko, and L. Savary, “Nematic insulator at charge neutrality in twisted bilayer graphene,” *arXiv:2008.05041*.
- [70] T. Soejima, D. E. Parker, N. Bultinck, J. Hauschild, and M. P. Zaletel, “Efficient simulation of moire materials using the density matrix renormalization group”, *Phys. Rev. B* **102**, 205111 (2020).
- [71] E. Khalaf, N. Bultinck, A. Vishwanath, and M. P. Zaletel, “Soft modes in magic angle twisted bilayer graphene”, *arXiv:2009.14827*.
- [72] A. Kumar, M. Xie, and A. H. MacDonald, “Lattice Collective Modes from a Continuum Model of Magic-Angle Twisted Bilayer Graphene”, *arXiv:2010.05946*.
- [73] S. Chatterjee, Matteo Ippoliti, Michael P. Zaletel, “Skyrmion Superconductivity: DMRG evidence for a topological route to superconductivity”, *arXiv:2010.01144*.
- [74] B.-B. Chen, Y. D. Liao, Z. Chen, O. Vafek, J. Kang, W. Li, Z. Y. Meng, “Realization of Topological Mott Insulator in a Twisted Bilayer Graphene Lattice Model”, *arXiv:2011.07602*.
- [75] D. E. Parker, T. Soejima, J. Hauschild, M. P. Zaletel, and N. Bultinck, “Strain-induced quantum phase transitions in magic angle graphene”, *arXiv:2012.09885*.
- [76] P. Potasz, M. Xie, and A. H. MacDonald, “Exact Diagonalization for Magic-Angle Twisted Bilayer Graphene”, *arXiv:2102.02256*.
- [77] J. M. Pizarro, M. Rösner, R. Thomale, R. Valentí, and T. O. Wehling, “Internal screening and dielectric engineering in magic-angle twisted bilayer graphene”, *Phys. Rev. B* **100**, 161102 (2019).
- [78] T. I. Vanhala and L. Pollet, “Constrained random phase approximation of the effective Coulomb interaction in lattice models of twisted bilayer graphene”, *Phys. Rev. B* **102**, 035154 (2020).
- [79] See Supplemental Material for the case with the variational method, the mass plot, and  $\mathbf{k}\cdot\mathbf{p}$  expansion.
- [80] Y. Ren, Q. Gao, A. H. MacDonald, and Q. Niu, “WKB estimate of bilayer graphene’s magic twist angles”, *Phys. Rev. Lett.* **126**, 016404 (2021).
- [81] S. Becker et al., “Mathematics of magic angles in a model of twisted bilayer graphene” *arXiv:2008.08489*.
- [82] O. Vafek and J. Kang, “Lattice model for the Coulomb interacting chiral limit of magic-angle twisted bilayer graphene: Symmetries, obstructions, and excitations”, *Phys. Rev. B* **104**, 075143 (2021)
- [83] N. Marzari, A. A. Mostofi, J. R. Yates, I. Souza, and D. Vanderbilt, “Maximally localized Wannier functions:



- Theory and applications”, *Rev. Mod. Phys.* **84**, 1419 (2012).
- [84] A. Abouelkomsan, Z. Liu, and E.J. Bergholtz, “Particle-Hole Duality, Emergent Fermi Liquids, and Fractional Chern Insulators in Moiré Flatbands”, *Phys. Rev. Lett.* **124**, 106803 (2020).
- [85] B. Tanatar and D. M. Ceperley, “Ground state of the two-dimensional electron gas”, *Phys. Rev. B* **39**, 5005 (1989).
- [86] B. Spivak and S. A. Kivelson, “Phases intermediate between a two-dimensional electron liquid and Wigner crystal”, *Phys. Rev. B* **70**, 155114 (2004).